High Marangoni number convection in a square cavity

A. Zebib

Department of Mechanical and Aerospace Engineering, Rutgers University, New Brunswick, New Jersey 08903

G. M. Homsy

Department of Chemical Engineering, Stanford University, Stanford, California 94305

E. Meiburg

Deutsche Forschungsund Versuchsanstalt für Luft und Raumfahrt, Gottingen, West Germany

The steady thermocapillary motion in a square cavity with a top free surface in the absence of gravitational forces is considered. The cavity is heated from the side with the vertical boundaries isothermal while the horizontal boundaries are adiabatic. The relative change in the surface tension is very small, i.e., an appropriate capillary number tends to zero, so that the free surface is assumed to remain flat at leading order. A finite-difference method is employed to compute the flow field. Numerically accurate solutions are obtained for a range of Prandtl numbers and for Reynolds numbers Re as high as 5×10^4. Surface deflections are computed as a domain perturbation for small capillary number. In addition, asymptotic methods are used to infer the boundary layer structure in the cavity, in the limit of large values of the Reynolds and Marangoni numbers. For a fixed Prandtl number Pr, it is shown that the Nusselt number, liquid circulation, and maximum vorticity are asymptotic to $Re^{1/3}$, $Re^{-1/3}$, and $Re^{2/3}$, respectively. These results are in agreement with the computed solutions. The leading-order solution for the free-surface deformation is sensitive to the value of Pr. With $Pr > 1$, the depression near the hot corner may exceed the elevation near the cold corner, while a secondary elevation may be induced near the hot corner when $Pr < 1$.

I. INTRODUCTION

Convective motions driven by a temperature gradient along the interface between two immiscible fluids caused by the variation of surface tension with temperature are of considerable interest and play an important role in small-scale and/or low-gravity hydrodynamics (Schwabe[1] and Ostrach[2]). Because these thermocapillary flows occur in crystal growth melts and dominate the convective flows in the micrograity environment of space, there have been a number of recent studies of simplified two-dimensional models with negligible gravitational effects.

Sen and Davis[3] consider steady thermocapillary convection in a differentially heated rectangular slot with a top free surface. They present results valid for vanishingly small aspect ratio A (height/width) with the Reynolds number $Re \sim O(A)$, the Marangoni number $Ma \sim O(A)$, and the capillary number $Ca \sim O(A^4)$. The same problem is also studied by Strani, Piva, and Graziani[4] for $A \to 0$ with $Ca \sim O(A^4)$ but with milder restrictions on Re and Ma. These studies are instructive in giving the flow field and surface deflection in a conduction-dominated regime, but give little information about strongly convective flows.

Strani *et al.*[4] also numerically compute the thermocapillary motions in a rectangular cavity with $A = 0.2$, 1, and 5 and with the Prandtl number $Pr = 1$ (i.e., $Ma = Re$). They allow for free-surface deformation and conclude, as expected, that for $Ca = 0.1$, surface deformations have a negligible influence on the flow field. Because they use a coarse mesh for their finite-difference computations, their results are accurate only for low Re and Ma. Since vigorous motion occurs in float zones at high values of Ma and Re, there is a

need for further study of this model problem. Axisymmetric modeling of a half-floating zone cofiguration has been considered by Fu and Ostrach[5] where they compute the flow field at different values of Re, Ma, and Pr. Many of the features of their solutions are common to ours, especially at high Ma, Re, for which a boundary layer regime develops.

The stability of such flows is of great interest. As the experiments of Preisser, Schwabe and Scharmann,[6] and Kamotani, Ostrach and Vargas[7] have shown, steady convection is stable only below certain values of the Marangoni numbers. Above the critical values, the flow is typically an oscillatory one, with commensurate changes in the transport properties and important implications in material processing applications. The only stability analysis of this class of flows is that of Smith and Davis,[8,9] who restricted their attention to plane-parallel flow profiles appropriate to conduction-dominated situations. It is not known how relevant the stability limits calculated by these authors are to strongly convective situations. We will see below that instabilities in cavities are more likely to be connected with the strong corner flows than with profiles of the type considered by Smith and Davis.[8,9]

In this paper we compute steady thermocapillary flows in a square cavity $(A = 1)$ by a finite-difference procedure. Our objective is to obtain accurate numerical solutions to the stated problem for as high a Reynolds number as possible, in order to characterize the nature of strongly convective flows of this general class. Only the case $Ca \to 0$ is considered, so that the free surface is assumed flat at leading order. Surface deflections are computed by domain perturbation. Boundary layer formation at different values of Pr is observed at large values of Ma and Re. We use the numerical results to

infer the relevant scalings of a consistent boundary layer picture of the flow, valid asymptotically as Re → ∞. We do not attempt to present a complete boundary layer theory since solving the boundary layer problem seems to be as difficult as solving the full equations of motion.

II. MATHEMATICAL MODEL

The physical model consists of a rectangular cavity of average height d and width w containing an incompressible, Newtonian liquid. The top horizontal boundary is a free surface open to a passive gas. The vertical rigid, isothermal walls are differentially heated and are kept at temperature $\pm T_0/2$ relative to an arbitrary reference temperature. The bottom boundary is rigid and adiabatic. In the absence of gravity, the nondimensional equations for the liquid motion are

$$\nabla \cdot \mathbf{V} = 0, \tag{1}$$

$$\text{Re } \nabla \cdot (\mathbf{VV}) = -\nabla p + \nabla^2 \mathbf{V}, \tag{2}$$

$$\text{Ma } \nabla \cdot (\mathbf{V}T) = \nabla^2 T. \tag{3}$$

Here length, velocity, temperature, and pressure are dimensionless with respect to d, $\gamma T_0/\mu$, T_0, and $\gamma T_0/d$, respectively, where μ is the viscosity and surface tension is assumed to decrease with temperature increase at a constant rate γ. The Reynolds number and the Marangoni numbers are defined in the usual way by

$$\text{Re} = d\gamma T_0/(\mu\nu), \tag{4}$$

$$\text{Ma} = \text{Re Pr}, \tag{5}$$

where ν is the kinematic viscosity, the Prandtl number $\text{Pr} = \nu/\kappa$, and κ is the thermal diffusivity.

The motion is referred to a Cartesian coordinate system with the origin at the middle of the bottom boundary with the y axis parallel to the side walls. The boundary conditions on the fixed surfaces are

$$\mathbf{V}(\pm 1/(2A),y) = 0, \tag{6a}$$

$$\mathbf{V}(x,0) = 0, \tag{6b}$$

$$T(\pm 1/(2A),y) = \mp \tfrac{1}{2}, \tag{7a}$$

$$T_y(x,0) = 0, \tag{7b}$$

where subscripts denote partial differentiation and the aspect ratio, $A = d/w$, which we set to unity in the remainder of this paper. The x and y components of $\mathbf{V}$ will be denoted as usual by u and v, respectively.

In addition to Re, Ma, and Pr, there is an additional dimensionless parameter which is a measure of the free surface deformation. This is the capillary number Ca and is given by

$$\text{Ca} = \gamma T_0/\sigma_0, \tag{8}$$

where σ_0 is an average value for the surface tension. We see that $\text{Ca} \sim \Delta\sigma/\sigma_0$, and in experiments is generally a small quantity (Kamotani et al.[7]). We thus consider the case $\text{Ca} \to 0$, i.e., only small variations in σ and in surface deformation are allowed. If, in addition to small Ca, we assume the contact angle is $\pi/2$, the surface is initially located at a height $y = 1$. Thus, to leading order in Ca, we assume a flat free surface with the boundary conditions

$$u_y(x,1) = -T_x(x,1), \tag{9a}$$

$$T_y(x,1) = 0. \tag{9b}$$

Corrections to the surface are computed as follows. If we denote the departure of the free surface from $y = 1$ by $h(x)$, then in the limit $\text{Ca} \to \infty$ we find from the normal stress balance,

$$h_{xx} = -\text{Ca } p, \tag{10a}$$

$$h(\pm \tfrac{1}{2}) = 0. \tag{10b}$$

Equation (10b) assumes a fixed contact line. Other boundary conditions are possible (Sen and Davis[3]). Because the pressure field $p(x,y)$ is determined only to an additive constant, an additional constraint on $h(x)$ from global continuity is

$$\int_{-1/2}^{1/2} h\, dx = 0. \tag{11}$$

Thus $h(x)$ can be determined to $O(\text{Ca})$ by solving (10) and (11) once p has been found. We note for future reference that the surface vorticity $\omega_s = -u_y(x,1)$ is simply the surface temperature gradient.

III. NUMERICAL PROCEDURE

Solutions to the system of equations (1)–(3),(6), (7), and (9) must be constructed by some numerical method. At a first glance it would seem that a spectral method with an infinite-order convergence (Gottleib and Orszag[10]) may be suited to the problem. However, the hot and cold corners on $y = 1$ are singular. The vorticity,

$$\omega = v_x - u_y, \tag{12}$$

is discontinuous at these corners, and will assume different values as a corner is approached on different paths. Indeed, following the local viscous analysis of Moffatt,[11] it can be shown that in the immediate vicinity of the hot corner, the vorticity is given by

$$\omega = -T_x(-1/2,1)(1 - 4\theta/\pi), \tag{13}$$

where the angle θ is 0 on $x = -\tfrac{1}{2}$ and $\pi/2$ on $y = 1$. It should be noted that the flow field corresponding to (13) is valid only very close to the corner so that the flow is locally a Stokes flow. A similar expression holds for ω near the cold corner. It is thus expected that ω will vanish on the diagonals as the corners are approached.

Since this discontinuity will limit the convergence of any spectral method, we opt for a finite difference approach. The method and the iteration procedure we use to solve the finite difference equations are described in detail by Patankar.[12] Briefly, the computational region is divided into rectangular control volumes with the grid points located at the geometric centers of these cells. Additional boundary grid points are included where the boundary conditions (6), (7), and (9) are imposed. The finite-difference equations are obtained by integrating the governing equations (1)–(3) over the control volumes with assumed local linear variations in any of the primitive variables. The convection and diffusion fluxes are approximated by a power-law scheme. Such a scheme accurately captures the nature of solutions to convective diffusion problems when diffusion is both strong and weak. Although any numerical scheme will have some diffusive errors be-

TABLE I. Influence of finite-difference grid on the solution.

Pr	Re	$M \times N$[a]	Nu_-	Nu_+	$-\psi_{max} \times 10^2$	$-\omega_{max}$
0.5	5×10^4	62×54	2.120	2.131	0.174	14.37
		70×60	2.161	2.151	0.180	14.44
0.1	5×10^4	62×54	2.937	2.957	0.168	29.04
		70×60	2.980	2.981	0.175	28.95
1	5×10^3	65×65	3.459	3.448	0.370	28.72
		80×80	3.454	3.447	0.373	31.20
		62×54	3.420	3.412	0.366	38.37
		70×60	3.428	3.425	0.369	38.35
1	5×10^2	62×54	4.895	4.898	0.155	139.4
		70×60	4.894	4.896	0.155	139.7

[a] Here M and N are the number of grid points in the x and y directions, respectively. The 65×65 and 80×80 grids are uniform while the 62×54 and the 70×60 grids are graded.

cause of the discretization, the one used here minimized this effect. The staggered location for the velocity components is adopted and the velocity-pressure coupling treatment (to enforce incompressibility) follows Patankar's revised procedure. A line-by-line iteration to solve the discretized equations is used with one completed iteration comprising five double sweeps of the field. Under-relaxation in solving for u, v, and T was required; a relaxation factor of 0.85 was used throughout. All computations were performed on a VAX 11/780. A converged solution requires from 250 to 450 iterations, with each iteration completed in less than 25 CPU seconds. Convergence was assumed when the largest variation in any of u, v, p, and T was less than some convergence tolerance which we set to 10^{-5}.

The accuracy of the results was assessed by mesh refinement studies. A number of solutions were computed on uniform grids with 65×65 and 80×80 mesh points. These solutions clearly indicated that at high Ma, Re, the dynamically significant boundary layers occur along the top surface and especially near the stagnation point at the cold boundary. We then refined the solutions using nonuniform grids, the first of which had 62 points in the x direction and 54 points in the y direction, with the finest mesh near the cold corner. The smallest volume at the cold corner is a square with mesh size 0.005. The rectangular cell at the hot corner is an x extent of 0.01. The mesh spacing was gradually increased away from the cold and hot corners in both the x and y directions. The largest mesh spacing near the middle of the bottom boundary is less than 0.05. We then used a nonuniform mesh with the same smallest elements, but with 70×60 points.

At high Re, it is clearly important to resolve all the length scales which are dynamically significant. We will see from the following that the smallest of these is $O(Re^{-2/3})$, with a leading constant which we cannot evaluate. With the 62×54 mesh, however, we do not expect much accuracy above $Re \sim 10^4$–10^5.

Table I shows the results of these mesh refinement studies. We show both local quantities such as the value of the circulation of the primary vortex ψ_{max} (here ψ is the stream function), and the maximum vorticity ω_{max}, as well as the more common global quantities, the Nusselt number (defined below in the usual way) for the hot and cold boundaries

Nu_- and Nu_+, respectively.

We first consider the results for $Pr = 1$. As can be seen from Table I, $Nu_+ = Nu_-$ to within a fraction of a percent, as must be because of the insulating conditions on the top and bottom walls. This agreement is an indication of the degree to which the numerical scheme is conservative. The error in the local quantities ψ_{max} and ω_{max} is estimated to be approximately 3%. A similar study of velocity and temperature profiles in the horizontal thermal layer along the top surface shows them to be spatially resolved to the same accuracy as the other local quantities. Similar considerations apply to the other cases shown in Table I. In particular, comparisons between the two graded meshes show the results for the 62×54 mesh to be essentially correct.

IV. NUMERICAL RESULTS; Pr = 1

Our primary interest is in the character of the motion at large values of Ma and Re. Equation (3) shows that Ma measures the strength of temperature (thermal energy) convection to diffusion. Thus large values of Ma will lead to the formation of thermal boundary layers. Equations (1) and (2) can be reduced to the vorticity transport equation

$$Re \, \nabla \cdot (V\omega) = \nabla^2 \omega, \qquad (14)$$

and hence large Re implies the formation of regions of concentrated vorticity, in particular near the free surface. We first consider the case $Pr = 1$, i.e., simultaneous formation of both temperature and vorticity layers with $Re = Ma$.

With $Pr = 1$, we compute the thermocapillary motion for $10^2 < Re < 10^4$. As expected, the flow consists of a major closed circulation, accompanied by corner eddies at the two lower corners. The temperature is distorted from a linear conductive field by this circulation, especially at high Ma. The surface temperature distribution is of key interest, since it is the gradient of this quantity which, through the thermocapillary stress, drives the motion. As an example of these features, we show in Figs. 1(a)–(c) the streamlines, isotherms, and isovorticity contours for $Re = Ma = 10^3$. As can be seen from Fig. 1(c), there is a large concentration of vorticity near the stagnation point at the cold (right) boundary. This is a result of the convective crowding of the isotherms into the stagnation point, as seen in Fig. 1(a). It is further seen that the stagnation point near the hot (left) boundary exhibits
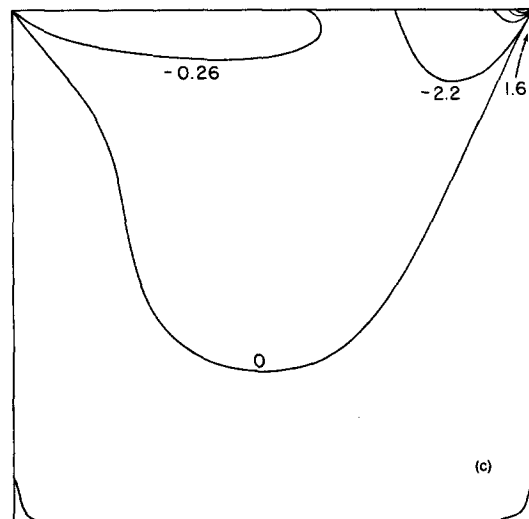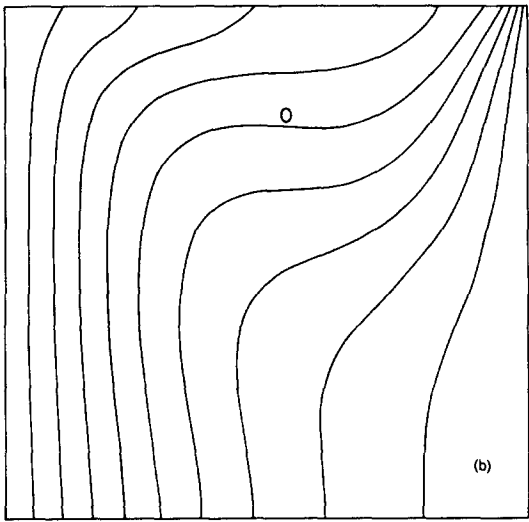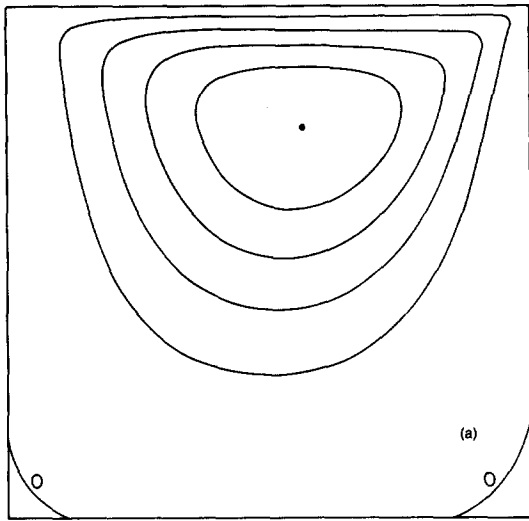
FIG. 1. Thermocapillary flow at $\mathrm{Pr} = 1$ and $\mathrm{Re} = 1000$. (a) Streamlines at equal increments of circulation. The motion is clockwise with $-\psi_{max} = 0.0048$. (b) Isotherms at equal increments. (c) Isovorticity contours. Here $\omega = -1.0$ and -11.79 at the top hot (left) and cold (right) corners, respectively. The largest positive value of ω is 7.3.
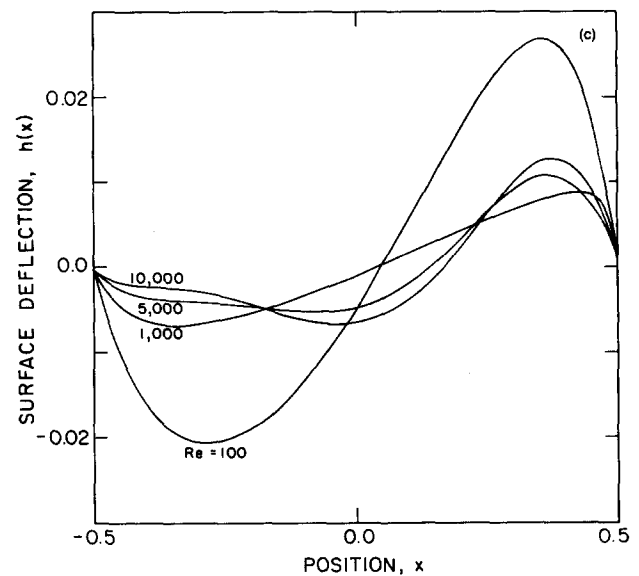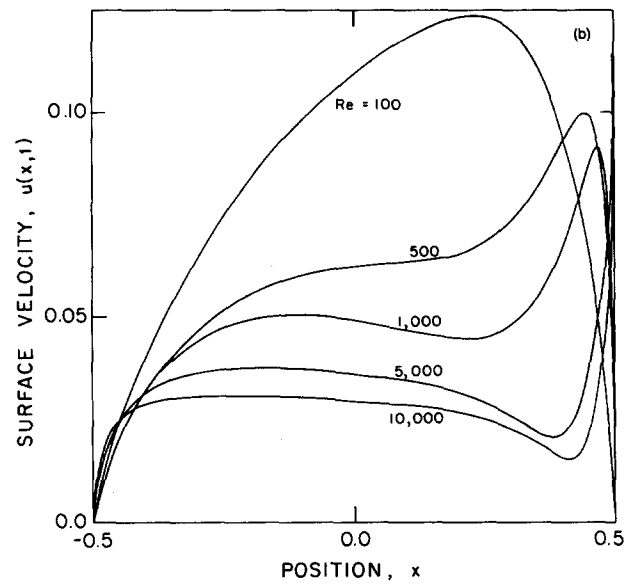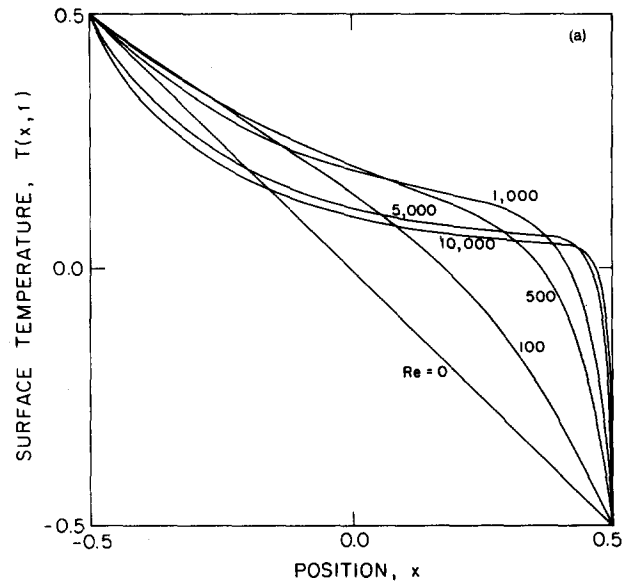

FIG. 2. Flow properties as a function of Reynolds number. (a) Surface temperature corresponding to $\mathrm{Pr} = 1$ and $\mathrm{Re} = 100$, 500, 1000, 5000, and $10\,000$. (b) Surface velocity. (c) Surface deflection.

little, if any, boundary layer behavior. The dividing $\omega = 0$ line is oriented at 45° near both stagnation points, as required by (13).

In Fig. 2 we show the results of our parametric study in Reynolds number. We plot surface temperature $T(x,1)$, velocity $u(x,1)$, and the surface deflection $h(x)$ for five different values of Re (or Ma). For Re less than about 1000, it is seen from Fig. 2(b) that the surface temperature gradient at the hot corner $T_x(-\frac{1}{2},1)$ is greater than the conduction value of -1, implying a decreased surface vorticity at the hot border. Figure 2(b) indicates that at relatively low values of Re, the surface velocity increases monotonically from zero and drops back smoothly to zero at the cold corner. The associated surface deflection plot in Fig. 2(c) shows that there are two peaks in $h(x)$ which decrease in magnitude and move toward the corners with increasing Re. With Re (or Ma) increasing above 1000, however, $T_x(-\frac{1}{2},1)$ is less than -1 and decreases with increasing Re, $u(x,1)$ exhibits two peaks, with $h(x)$ showing a more less flat depression on an increasing length of the free surface near the hot (left) boundary. It is also observed that the surface elevation near the cold corner increases with Re. From these features it may be concluded that a boundary layer regime begins to develop for Re (or Ma) greater than about 1000.

The streamlines, vorticity, and temperature fields corresponding to $Re = Ma = 10^4$ are shown in Fig. 3. These results suggest that the limiting flow field at large values of Re (or Ma) will consist of an isothermal core of constant vorticity, with boundary layers forming on the four boundaries. Note that the vorticity is again discontinuous near the two upper corners in accord with Eq. (13). The sharpest gradients occur near the cold corner as is evident in Fig. 3(c).

Of interest is the total heat transport, or the Nusselt number, defined by

$$\mathrm{Nu}_\pm = \int_0^1 -T_x(\pm\tfrac{1}{2},y)dy. \tag{15}$$

As noted above, $\mathrm{Nu}_+ = \mathrm{Nu}_-$ to within 1%.

V. STRUCTURE OF BOUNDARY LAYERS; $Pr = O(1)$

We develop a self-consistent picture of the boundary layer structure which exists asymptotically as $\mathrm{Re} \to \infty$. We show that, beginning with the key assumption that the free surface vorticity becomes independent of Re as $\mathrm{Re} \to \infty$, all of the available numerical evidence is in agreement with the scalings which are implied by such an assumption.

We first give a discussion of the assumption on which our boundary layer scalings are based. As $\mathrm{Re} \to \infty$, there are two possibilities for the surface temperature distribution: either the surface becomes isothermal because of the effects of strong surface convection, or the surface temperature gradient remains $O(1)$ (equivalently, the surface vorticity approaches a constant). These two possibilities imply a different structure for the flow as $\mathrm{Ma} \to \infty$. In the first case, the surface temperature gradients are confined to small regions near the stagnation points on the hot and cold boundaries. Gradients will necessarily occur over a lateral distance of
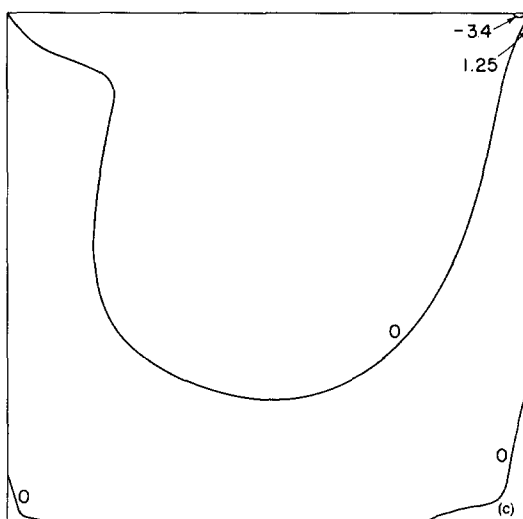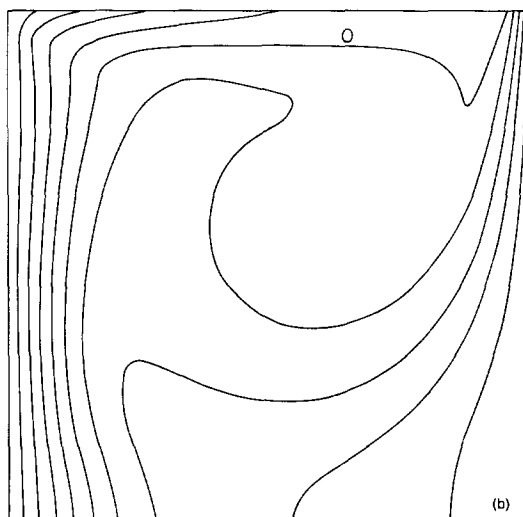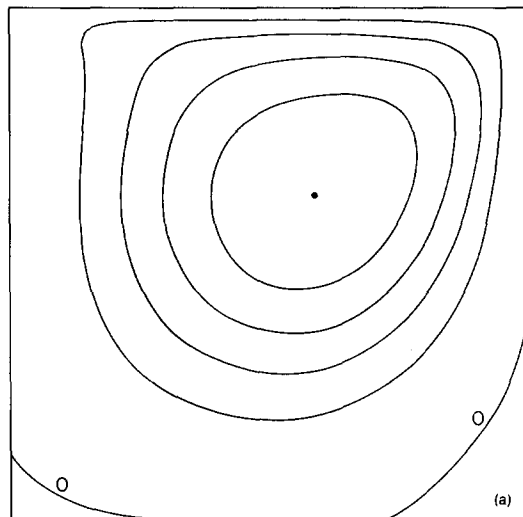

FIG. 3. Same as Fig. 1 but with Re = 10 000. Here $-\psi_{max} = 0.003$; $\omega = -2.4$ and -60.2 at the top hot and cold corners, respectively; and the largest positive value of ω is 10.5.

$O(1/\text{Re})$, implying that the surface vorticity is a maximum near the corner, with

$$\omega_{\max} \sim T_x \sim O(1/\text{Re}). \tag{16}$$

The circulation would then be driven by this local concentration of vorticity, and could possibly have enough inertia to sustain a closed circulation strong enough to cause the surface to remain isothermal. Consistent with (16) is the prediction that the surface velocity

$$u(x,1) \sim O(1) \tag{17}$$

uniformly in x as Ma $\rightarrow \infty$. This uniformity is not seen in the results shown in Fig. 2(b). As we will see below, the scalings (16) and (17) are not supported by the numerical results.

Consider the second alternative that the surface temperature gradient and surface vorticity remain $O(1)$ over most of the surface. This is a plausible assumption if we picture the circulation as being driven by a thermocapillary stress over most of the surface, as opposed to being driven by a vorticity source in small regions near the corners. This second alternative is suggested by the results in Fig. 2(a) and results in scalings which are rather different from (16) and (17). We now proceed to develop these scalings, which involves more detailed arguments than those necessary to arrive at (16) and (17), but yields more detailed estimates of the dependence of properties of the flow upon Re.

A. Free surface layer

The first region of interest is the boundary layer near the free surface. Here $x \sim O(1)$. The assumption $\omega \sim O(1)$, together with the required balance of diffusion and convection, leads to the free surface scalings:

$$x = \bar{x}, \tag{18a}$$

$$y = 1 - \text{Re}^{-1/3} \, \bar{y}, \tag{18b}$$

$$u = \text{Re}^{-1/3} \, \bar{u}(\bar{x},\bar{y}), \tag{18c}$$

$$v = - \text{Re}^{-2/3} \, \bar{v}(\bar{x},\bar{y}), \tag{18d}$$

$$\psi = \text{Re}^{-2/3} \, \bar{\psi}(\bar{x},\bar{y}), \tag{18e}$$

$$T = \bar{T}(\bar{x},\bar{y}). \tag{18f}$$

Equation (18c) implies a surface velocity decreasing with Re in agreement with Fig. 2(b). We wish to determine the appropriate pressure scale for the free surface layer. The usual boundary layer arguments [see (19c) below] indicate that this pressure scale must be consistent with that in the core. The core scalings are discussed below, but at this point it is possible to state that if the free surface layer is at all affected by pressure gradients associated with the core flow we must have

$$\max(p) \sim O(\text{Re}^{1/3}). \tag{18g}$$

Thus we set

$$p = \text{Re}^{1/3} \, \bar{p}(\bar{x},\bar{y}). \tag{18h}$$

The boundary layer equations to leading order become

$$\bar{u}_{\bar{x}} + \bar{v}_{\bar{y}} = 0, \tag{19a}$$

$$\bar{u}\bar{u}_{\bar{x}} + \bar{v}\bar{u}_{\bar{y}} = - \bar{p}_{\bar{x}} + \bar{u}_{\bar{y}\bar{y}}, \tag{19b}$$

$$0 = \bar{p}_{y}, \tag{19c}$$

$$\bar{u}\bar{T}_{\bar{x}} + \bar{v}\bar{T}_{\bar{y}} = \text{Pr}^{-1} \, \bar{T}_{\bar{y}\bar{y}}. \tag{19d}$$

These are the usual boundary layer equations. The known boundary conditions are

$$\bar{y} = 0, \quad \bar{v} = \bar{T}_{\bar{y}} = 0, \tag{20a}$$

$$- \bar{u}_{\bar{y}} = \bar{T}_{\bar{x}}. \tag{20b}$$

Matching conditions for $\bar{y} \rightarrow \infty$ with a core solution (which is in general a function of x) and initial conditions for $\bar{x} \rightarrow -\frac{1}{2}$ must be provided.

B. Core region

Formally, the limiting equations in the core are

$$(\mathbf{V} \cdot \nabla)\omega = 0, \tag{21a}$$

$$(\mathbf{V} \cdot \nabla)T = 0. \tag{21b}$$

Thus, in principle, ω and T are constants along streamlines, and if the streamlines are closed in regions removed from boundaries, T and ω must be constant. Figure 2(b) and (c) suggests that the limiting core flow is isothermal and of constant vorticity. The strength of the circulation may be determined by observing that the velocity $u(x,y)$ must match between the core and the free surface layer. Since $x,y \sim O(1)$ in the core, and $\bar{u} \sim O(\text{Re}^{-1/3})$ in the free surface layer,

$$\psi_{\text{core}} \sim O(\text{Re}^{-1/3}) \tag{22}$$

is the only scaling consistent with the matching condition. We can also show that this scaling leads to internally consistent pressure scalings. Since the core vorticity is constant, the Bernoulli relation,

$$p + \text{Re}|q^2|/2 \simeq \text{const}, \tag{23}$$

must hold, where q is the speed of the core circulation. Since $q \sim O(\text{Re}^{-1/3})$, we find that

$$p \sim O(\text{Re}^{1/3}), \tag{24}$$

consistent with that allowed by the boundary layer scalings (18g) and (18c). Thus, $\bar{p}(\bar{x})$ is simply the core pressure field $p(x,y)$ evaluated at $y = 1$.

C. Cold corner region

This stagnation point flow region is where most of the heat transfer on the cold boundary occurs and where the largest vorticity is generated [Figs. 2(a) and 3(c)]. The horizontal free surface flow turns in this region as $u(x,1)$ drops sharply to zero [Fig. 2(b)]. The y extent and the flux of fluid in this region are determined by the corresponding quantities in the free surface region. Thus, this turning flow is assumed to take place over a vertical extent of $O(\text{Re}^{-1/3})$, with a fluid flux of $(\text{Re}^{-2/3})$. In addition, the required convection-diffusion balance leads to the cold corner scalings

3472   Phys. Fluids, Vol. 28, No. 12, December 1985

Zebib, Homsy, and Meiburg   3472

$$y = 1 - \mathrm{Re}^{-1/3}\, \tilde{y}, \tag{25a}$$

$$x = \tfrac{1}{2} - \mathrm{Re}^{-2/3}\tilde{x}, \tag{25b}$$

$$u = -\mathrm{Re}^{-1/3}\, \tilde{u}(\tilde{x},\tilde{y}), \tag{25c}$$

$$v = -\tilde{v}(\tilde{x},\tilde{y}), \tag{25d}$$

$$\psi = \mathrm{Re}^{-2/3}\, \tilde{\psi}(\tilde{x},\tilde{y}), \tag{25e}$$

$$\omega = \mathrm{Re}^{2/3}\, \tilde{\omega}(\tilde{x},\tilde{y}), \tag{25f}$$

$$p = \mathrm{Re}^{1/3}\, \tilde{p}(\tilde{x},\tilde{y}), \tag{25g}$$

$$T = \tilde{T}(\tilde{x},\tilde{y}). \tag{25h}$$

The leading-order equations, boundary, and matching conditions become

$$\tilde{u}_{\tilde{x}} + \tilde{v}_{\tilde{y}} = 0, \tag{26a}$$

$$\tilde{u}\tilde{u}_{\tilde{x}} + \tilde{v}\tilde{u}_{\tilde{y}} = -\tilde{p}_{\tilde{x}} + \tilde{u}_{\tilde{x}\tilde{x}}, \tag{26b}$$

$$\tilde{u}\tilde{v}_{\tilde{x}} + \tilde{v}\tilde{v}_{\tilde{y}} = \tilde{v}_{\tilde{x}\tilde{x}}, \tag{26c}$$

$$\tilde{u}\tilde{T}_{\tilde{x}} + \tilde{v}\tilde{T}_{\tilde{y}} = \mathrm{Pr}^{-1}\, \tilde{T}_{\tilde{x}\tilde{x}}, \tag{26d}$$

$$\tilde{x} = 0; \quad \tilde{u} = \tilde{v} = 0, \tag{26e}$$

$$\tilde{T} = -\tfrac{1}{2}, \tag{26f}$$

$$\tilde{x} \rightarrow \infty; \quad \tilde{v} \rightarrow 0, \tag{26g}$$

$$\tilde{u}(\tilde{x} \rightarrow \infty,\tilde{y}) \sim -\bar{u}(\bar{x} \rightarrow \tfrac{1}{2},\bar{y}). \tag{26h}$$

These quantities cannot satisfy initial conditions on $\bar{y} = 0$ since $\bar{u}_{\bar{y}} \sim O(1)$ while $\tilde{T}_{\tilde{x}} \sim O(\mathrm{Re}^{2/3})$. Thus, there will be corner subregions in which effects of viscosity and conduction will be included as one moves to smaller and smaller scales. The key dynamic behavior in this region is captured, however, by scales which allow the x-directed flow $\bar{u}(\tilde{x},\tilde{y})$ to meet the stagnation region and turn to a y-directed flow, $\tilde{v}(\tilde{x},\tilde{y})$. The requirement that this turning flow be viscous in the x direction and carry the same volume flux as the top layer then sets the scales for $\tilde{x}$ and $\tilde{\omega}$. Thus the corner subregions mentioned above have little dynamic significance. This situation is similar to problems in rotating flows and buoyancy-driven convection in which small corner regions having viscous scales exist, but do not participate in a key way in the transport; see e.g., Hunter,[13] Homsy and Hudson,[14] Walker and Homsy.[15] It is easy to show that dropping the requirement that the turning flow is viscous, i.e., considering a purely inertial, convective flow, leads to a scaling $\tilde{x} \sim O(1)$, $\tilde{\omega} \sim O(1)$ that obviously contradicts the assumed boundary layer nature of the flow.

D. Rigid wall scalings

Solutions to the core equations will not, of course, satisfy the boundary conditions on the rigid walls, thus necessitating the occurrence of conventional $O(\mathrm{Re}^{-1/2})$ layers. We argue that these too are of secondary importance in determining the transport. Since the entire flow is driven by the nonisothermal surface, as we have shown, large velocities are confined to the free surface layer and the cold corner region, respectively. These in turn drive a core circulation, the scaled strength of which *decreases* as Re increases [cf. Eq. (22)]. Thus, these $O(\mathrm{Re}^{-1/2})$ boundary layers can be de-

TABLE II. Numerical results for Pr = 1.

$\mathrm{Re} \times 10^{-3}$	Nu_+	Nu_-	$\psi_{\mathrm{max}} \times 10^2$	$-\omega_{\mathrm{max}}$
1	1.93	1.92	0.479	11.8
2	2.47	2.47	0.424	20.2
3	2.86	2.85	0.404	26.8
4	3.17	3.16	0.384	32.8
5	3.42	3.41	0.366	38.4
6	3.65	3.63	0.350	43.5
7	3.85	3.83	0.337	48.2
8	4.03	4.01	0.326	52.5
9	4.19	4.17	0.315	56.5
10	4.34	4.32	0.305	60.2

termined, in principle, as an *a posteriori* correction to the core flow.

E. Comparison with numerical results

The asymptotic scalings we have inferred make certain predictions which can be compared against our numerical results at large but finite Re. The first pertains to the mean heat transport, or the Nusselt number. From the scalings in the cold wall region, we find

$$\tilde{T} \sim O(1), \quad \tilde{x} - \tfrac{1}{2} \sim O(\mathrm{Re}^{-2/3}).$$

It follows that most of the heat flux to the cold wall occurs in this corner region. Specifically, we find

$$\mathrm{Nu}_+ \equiv \int_0^1 -T_x\left(\tfrac{1}{2},y\right)dy \sim \mathrm{Re}^{1/3} \int_0^\infty \tilde{T}_{\tilde{x}}(0,\tilde{y})d\tilde{y}$$
$$\sim O(\mathrm{Re}^{1/3}). \tag{27}$$

Numerical evaluation of the local heat flux along the cold boundaries shows that indeed, most of the heat transfer occurs near the cold stagnation point. This contrasts with the heat flux distributions along the hot wall, which are evenly distributed. The scaling (27) is consistent with the convective energy flux carried by the free surface layer, which is

$$\mathrm{Re} \int^{\bar{y}} \bar{u}\bar{T}_x \, d\bar{y} \sim O(\mathrm{Re}^{1/3}). \tag{28}$$

Other predictions are that the maximum vorticity will occur in this cold corner region, with

$$\tilde{\omega}_{\mathrm{max}} \sim \tilde{T}_{\tilde{y}} \sim O(\mathrm{Re}^{2/3}), \tag{29}$$

and the strength of the circulation in the core is

$$\psi \sim O(\mathrm{Re}^{-1/3}). \tag{30}$$

Quantitative evidence for the correctness of this boundary layer structure comes from examining the computed values of $\mathrm{Nu} = (\mathrm{Nu}_+ + \mathrm{Nu}_-)/2$, ψ_{max}, ω_{max}. Numerical values of these quantities are given in Table II. Figure 4 shows a logarithmic plot of these data for all the cases with Pr = 1 that we have computed. From this figure we conclude that our computed solutions for large but finite Re support the asymptotic scalings inferred above, but that boundary layer behavior is not reached until Re is between 5×10^3 and 10^4. We also comment that this structure, while valid for Pr = 1, may be substantially altered from extreme values of Pr. Figure 5 gives a schematic summary of the structure for Pr = 1.
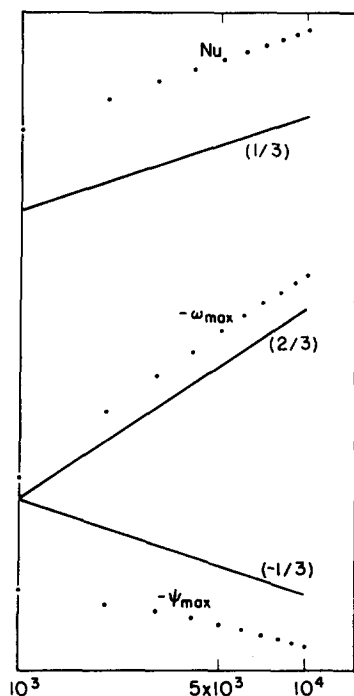
FIG. 4. Variation with log Re of log $(-\psi_{max})$, log$(-\omega_{max})$, and log Nu. Also shown are straight lines with slopes $-\frac{1}{3}$, $\frac{2}{3}$, and $\frac{1}{3}$.

VI. NUMERICAL RESULTS: Pr $\neq$ 1

Equations (3) and (4) show that convection of vorticity is stronger (weaker) than convection of energy according to Pr < 1 (Pr > 1). The influence of Pr on the motion is ascer-
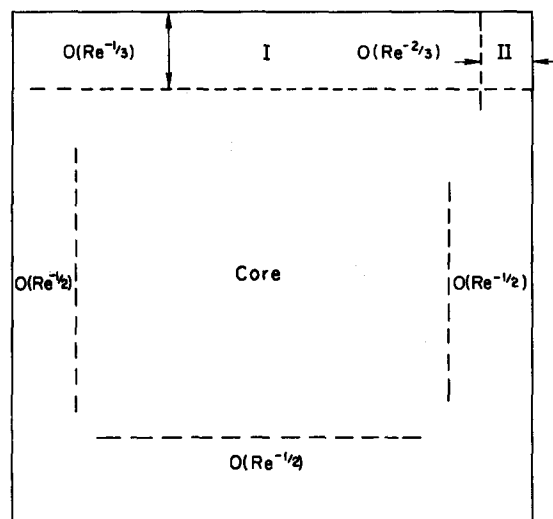

FIG. 5. Sketch of the important boundary layer regions. The following are the scalings in regions I, II, and the core.

	u	v	ψ	ω	T_x
I	$Re^{-1/3}$	$Re^{-2/3}$	$Re^{-2/3}$	1	1
II	$Re^{-1/3}$	1	$Re^{-2/3}$	$Re^{2/3}$	$Re^{2/3}$
core	$Re^{-1/3}$	$Re^{-1/3}$	$Re^{-1/3}$	1	1
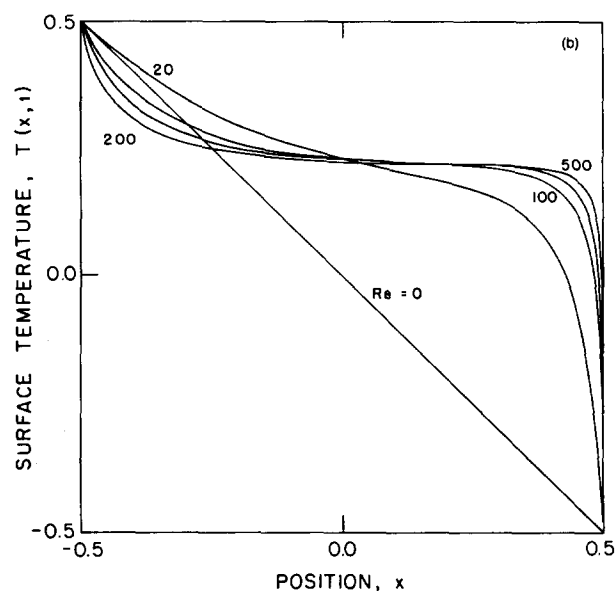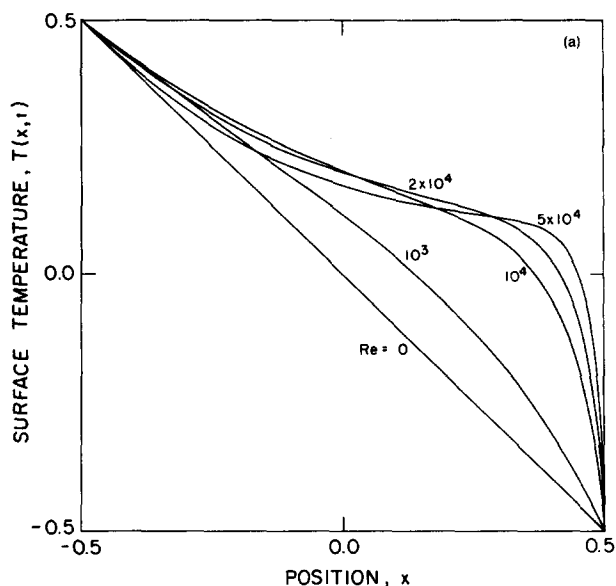
FIG. 6. Surface temperature $T(x,1)$ at (a) Pr = 0.1 and Re = 10^3, 10^4, 2×10^4, and 5×10^4. (b) Pr = 50 and Re = 20, 100, 200, and 500.

tained from a sequence of computations with Pr = 0.05, 0.1, 1, 10, and 50. The largest value of Re or Ma attainable with reasonable accuracy was 5×10^4.

Figures 6(a) and (b) are plots of the surface temperature corresponding to Pr = 0.1 and 50 at various values of Re. It is seen that, with increasing Re, the surface vorticity at the hot corner first decreases, and then begins to increase monotonically with further increase in Re. This is similar to the case Pr = 1 in Fig. 2(a). The surface velocity corresponding to the parameter values of Fig. 6(a) and (b) are shown in Fig. 7(a) and (b). It is observed that a two-peak structure is eventually approached at sufficiently large Re (or Ma). It is important to note [Fig. 7(b)] that at appropriately low values of Re (depending on Pr), for Pr > 1 the motion is faster near the hot corner than almost everywhere on the free surface except in the readily developed thermal layer (and vorticity layer at the cold corner). The opposite is true for Pr < 1 and low Re,

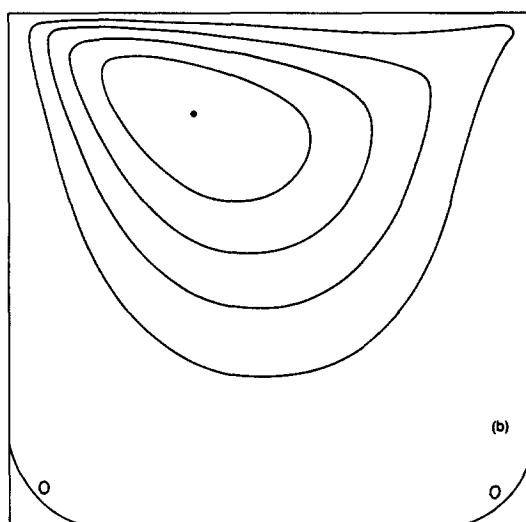FIG. 7. Associated surface velocity $u(x,1)$ at the parameter values of Fig. 6(a) and (b), respectively.
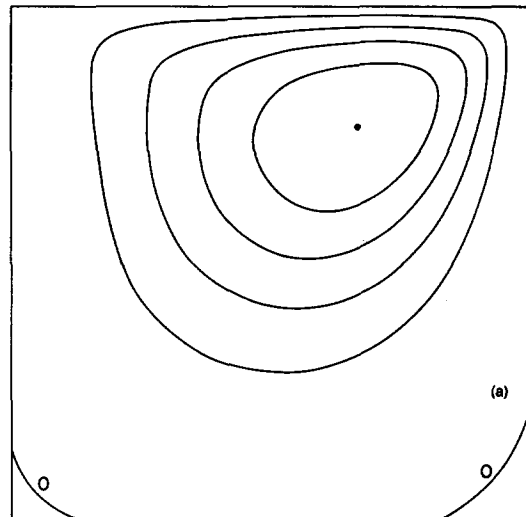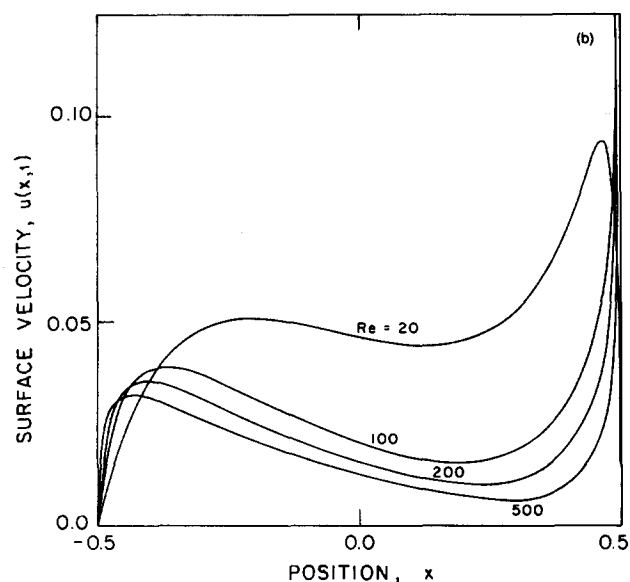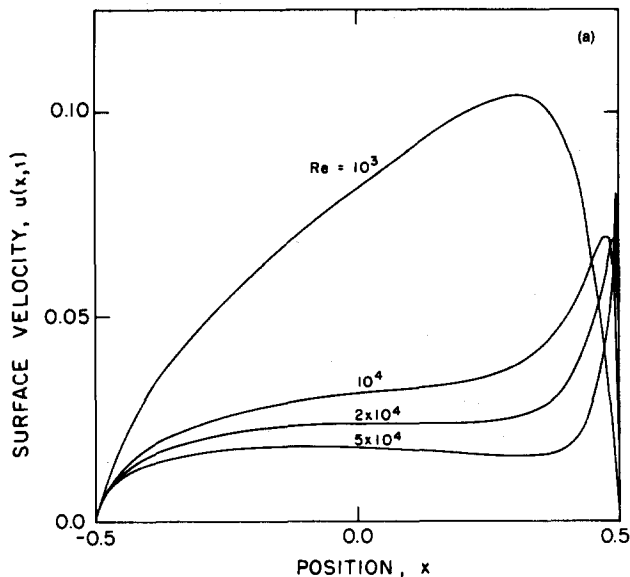

FIG. 8. Streamlines corresponding to (a) $Pr = 0.05$ and $Re = 1000$; $-\psi_{max} = 0.0088$, and (b) $Pr = 50$ and $Re = 200$; $-\psi_{max} = 0.0019$.

see Fig. 7(a), where convection is expected to dominate near the cold corner.

The influence of Pr on the pattern of circulation is evident from Fig. 8(a) and (b) which show the streamlines of the thermocapillary motion corresponding to Pr, Re, and Ma values of 0.05, 1000, 50, and 50, 200, 10 000. At sufficiently low Re it is seen that the point where ψ_{max} occurs is close to the cold corner when $Pr < 1$, while for $Pr > 1$ this point occurs near the hot corner. Thus, it is again concluded that convective effects are more important at the hot (cold) corner according or $Pr > 1$ (< 1) at appropriate low values of Re. With increasing Re, however, the pattern of motion is similar to that for $Pr = 1$ in Fig. 3(a). This behavior with Pr was also found by Fu and Ostrach[5] in their axisymmetric half-zone model.

The most remarkable influence on Pr on thermocapillary convection is found on the shape of the free surface. Figures 9(a) and (b) show $h(x)$ for the parameter values in Figs. 6(a) and (b) and 7(a) and (b). It is seen that for $Pr > 1$, the region of strong motion near the hot corner is accompanied by sufficient low pressure that the largest depression exceeds the largest elevation. At $Pr < 1$, however, there is a buildup of pressure sufficient to produce a secondary elevation near the hot corner.

It is of interest to note that, for all the cases considered, $|h(x)|$ is small, indicating that the range of capillary numbers for which the surface deflection is accurately given by perturbation in Ca may be rather large.

VII. CONCLUSIONS

We have presented the results of a reasonably complete study of thermocapillary convection in a square cavity. Our
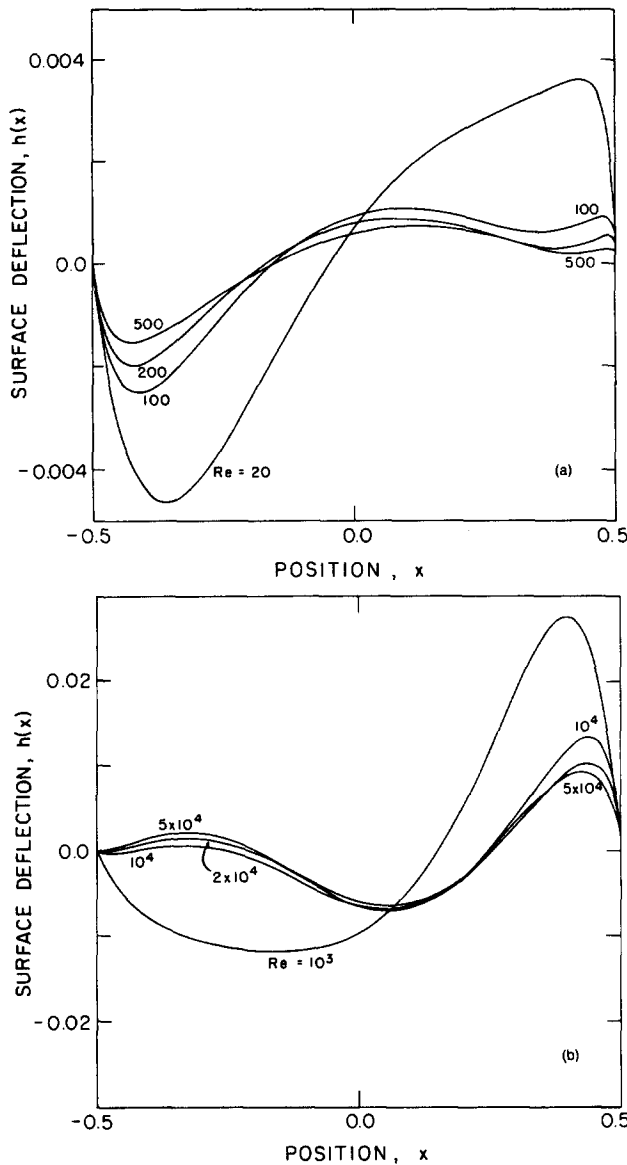
FIG. 9. Surface deflection at the parameter values of Fig. 6(a) and (b), respectively.

accurate computational procedure allows us to consider situations with large Re and Ma, and thus observe the forma-

tion of boundary layers, in particular at the cold stagnation point region. This boundary layer structure is shown to be consistent with an asymptotic theory valid as Re → ∞.

We encountered no difficulty in computing two-dimensional steady states by time-like iterations. It is also felt, from numerical experiments, that such steady motion continue to exist at yet higher values of Re and Ma. Since, from previous experimental work and from the analysis of Smith and Davis,[8,9] it is expected that oscillatory motions will occur at some critical Re and Ma, it is conjectured that such an unsteady motion is three-dimensional. Furthermore, our results at finite Ma in a finite cavity suggest that experimentally observed instabilities may be associated with the rapid turning flows and high vorticity associated with the cold wall region, as opposed to the parallel shear flows treated by Smith and Davis.

ACKNOWLEDGMENTS

[1]D. Schwabe, Physiochem. Hydrodyn. **2**, 263 (1981).
[2]S. Ostrach, Ann. Rev. Fluid Mech. **14**, 313 (1982).
[3]A. K. Sen and S. H. Davis, J. Fluid Mech. **121**, 163 (1982).
[4]M. Strani, R. Piva, and G. Graziania, J. Fluid Mech. **130**, 347 (1983).
[5]B. Fu and S. Ostrach, *Proceedings of the* ASME *Winter Meeting*, Boston, Massachusetts, November 13–18, 1983 (American Society of Mechanical Engineers, New York, 1983), p. 1.
[6]F. Preisser, D. Schwabe, and A. J. Scharmann, Fluid Mech. **126**, 545 (1983).
[7]Y. Kamotani, S. Ostrach, and M. Vargas, J. Crystal Growth **66**, 83 (1984).
[8]M. K. Smith and S. H. Davis, J. Fluid Mech. **132**, 119 (1983).
[9]M. K. Smith and S. H. Davis, J. Fluid Mech. **132**, 145 (1983).
[10]D. Gottlieb and S. Orszag, *Numerical Analysis of Spectral Methods: Theory and Applications* (Society for Industrial and Applied Mathematics, Philadelphia, 1977).
[11]H. K. Moffatt, J. Fluid Mech. **18**, 1 (1964).
[12]S. V. Patankar, Numer. Heat Transfer **4**, 409 (1981).
[13]C. Hunter, J. Fluid Mech. **27**, 753 (1967).
[14]G. M. Homsy and J. L. Hudson, J. Fluid Mech. **35**, 33 (1969).
[15]K. L. Walker and G. M. Homsy, J. Fluid Mech. **87**, 449 (1978).

3476   Phys. Fluids, Vol. 28, No. 12, December 1985

Zebib, Homsy, and Meiburg   3476